From Darkness to Light
ASP Conference Series, Vol. 243, 2001
T. Montmerle & Ph. André, eds.

Dynamical Structure in HST/NICMOS Images of Nearby Protostars

Susan Terebey, Dave Van Buren, Terry Hancock

Extrasolar Research Corporation,
Pasadena, CA 91101, USA

Deborah L. Padgett and Michael Brundage

Jet Propulsion Laboratory, Pasadena, CA 91125, USA

Abstract. We present near-infrared images of class I protostars in the Taurus and ρ Ophiuchus molecular clouds made with the NICMOS camera on the Hubble Space Telescope. The HST/NICMOS data provide striking images of protostars and give a new window onto the gravitational collapse phase. The high spatial resolution of 0.15″ (20 AU) reveals the full complexity of dynamical collapse: binary protostars surrounded by nebulosity; the nebulosity showing streamers of material infalling into the central regions, dust disks seen in absorption, and disks oriented at odd angles with respect to the large scale outflow. Two protobinary systems are discovered in eight objects observed, IRS44 (IRAS16244-2432) and TMR-1 (IRAS04361+2547), both with $0.3'' \sim 45$ AU separation. A protostar in nearby TMC1 (IRAS04381+2540) displays both a wide-angle outflow and a jet, thus providing a unifying link between protostars and Herbig-Haro jet sources.

Keywords: ISM: Gravitational Collapse - Cores: Protostellar - Stars: Formation, Binaries, Protobinaries, Outflows, Disks - Regions: Taurus, Ophiuchus - Objects: TMR-1, TMC1, TMC1A, IRAS 04169, IRS43, IRS44 - Instruments: HST

1. Introduction

In broad outline, the paradigm for the formation of isolated low-mass stars (Shu, Adams, & Lizano 1987) starts with the formation of dense quiescent cloud cores in molecular clouds over a $10^6 - 10^7$ yr timescale. A core may fragment to form several stars. When sufficiently centrally concentrated the dense core begins to collapse. The basic structure of protostar plus disk, surrounded by dense infalling envelope and rarefied bipolar outflow is quickly established and persists over the few by 10^5 years it takes for the protostar to accrete its final mass. Illustrating the paradigm on small spatial scales are WFPC2 images of the edge-on disk system HH30 which show a dust disk in absorption whose edges are illuminated by scattered light (Burrows et al. 1996). Ground-based NIR images of IRAS04302+2247 show an edge-on view of a younger source (Lucas & Roche 1997; Padgett et al. 1999). Bontemps et al. (1996) investigate

an age/evolutionary sequence based on circumstellar mass, where the growing protostar is a mass "sink" for the collapsing cloud core (see also André et al., this volume). Padgett et al. (1999) studied six objects with HST/NICMOS spanning the transition ($10^5 - 10^6$ yr) from protostar to TTauri star. When ordered by circumstellar mass they find the near-infrared structure changes in appearance from envelope-dominated (i.e. young), to disk-dominated (i.e. older). Binaries however present a challenge to this age scheme because of their systematically lower disk masses (Osterloh & Beckwith 1995).

Despite the prevalence of binary systems, our understanding of their formation is less advanced (see reviews by Bodenheimer, Ruzmaikina, & Mathieu 1993; Boss 1995). Binaries with wide separations (> 100 AU) are easily explained, but collapse calculations show the initial conditions for small binary separations require low-mass fragments, fragments whose masses are small compared with final stellar masses (Boss 1986; Bonnell & Bate 1994). As a consequence, binary formation studies have increasingly focused on the collapse phase, investigating the question of how multiple stars might form from 'seed masses' which accrete and grow and possibly merge during the protostellar collapse phase (Bate 1997; also Bate, this volume).

These considerations suggest that observations of circumstellar environments during the protostar phase may reveal density inhomogeneities, nonaxisymmetric structures, or other evidence of dynamical collapse processes. Near-infrared images are sensitive to structure which arises within the infall envelope or circumstellar disk. This may include outflow related structures such as wind-swept shells. It can also include density inhomogeneities related to collapse processes and binary formation. The HST/NICMOS spatial resolution of $\sim 0.15''$ corresponds to 20 – 25 AU in the nearest molecular clouds. This resolves circumstellar disks ($\sim$ 100 AU), permitting the study of circumstellar disks as well as their influence on binary star formation.

This paper presents near-infrared imaging of the circumstellar environments of class I young stellar objects (YSO; Lada 1987). The class I sources are thought to show low-mass protostars during the main gravitational collapse phase. Over a typical scale of $3'' \sim 500$ AU the data show material which is dynamic rather than static, namely gas that is in motion, whether due to collapse, outflow, or rotation. To illustrate, a self-gravitating cloud which is pressure supported will approximately satisfy $GM/r = a^2$; further assuming 1 M$\odot$ within 500 AU radius then implies $a \sim 1.3$ km s^{-1} for the equilibrium gas sound speed required to support the cloud. However collapse calculations show cloud collapse is nearly isothermal, so that the sound speed changes little from ~ 0.3 km s^{-1} initial values. Thus, at 500 AU, the circumstellar material cannot be pressure supported. In fact, the $T \sim 400$ K temperature needed in this example for thermal pressure support at 500 AU is only achieved on much smaller scales, $r \sim 1$ AU for a 1 L$\odot$ YSO. Observations confirm the dense gas is cold on small scales, with interferometer observations of Class I protostars in Taurus finding gas kinetic temperatures ranging from 25 - 80 K inside 1000 AU (Hogerheijde et al. 1998).

Ground-based NIR imaging studies have established that the extended NIR emission around protostars is primarily due to scattered light (Heyer et al. 1990). Monte Carlo radiative transfer models have had good success in matching observed NIR images (Whitney & Hartmann 1993; Whitney, Kenyon, & Gomez

1997). The observed (bi)conical structure is produced by a combination of the infall envelope, the circumstellar disk, and the cavity evacuated by a bipolar outflow. Stellar photons traverse the outflow cavity and are then absorbed or scattered in the dusty disk or in the infall envelope. The resultant images reveal the $\tau \sim 1$ scattering surface, providing a direct way to measure the dust column and infer the density of the disk and infall envelope.

2. Sample and Observations

Sources were selected to be nearby protostars and known from ground-based imaging to have strong extended NIR emission. The Taurus sources are representative of the isolated mode of star formation. The Ophiuchus sources fall within the higher density environment of the ρ Oph embedded cluster. All objects are classified as class I protostars, except S2 in ρ Oph which has been classified as a flat spectrum class II (star plus disk). Table 1 shows source parameters.

Table 1. Protostar Sample and Source Parameters.

YSO Name	Core	Dist(pc)	$L/L_{\odot}^{a}$	SED[a]	J[b]	H[b]	K[b]
IRAS04169+2702	B213	140	1.4	I	>16.4	14.2	11.4
IRAS04361+2547	TMR-1	140	3.8	I	16.2	12.8	10.6
IRAS04365+2535	TMC1A	140	2.4	I	17.1	13.3	10.5
IRAS04381+2540	TMC1	140	0.7	I	>16.1	14.5	12.1
S2/GSS32	OphA	160	4.9	IID	10.8	8.7	7.2
EL29	L1681B/OphF	160	41.0	I	17.2	12.0	7.5
IRS43	OphE	160	10.1	I	>17.0	13.2	9.5
IRS44	L1681B/OphF	160	13.0	I	>17.0	13.1	9.6

[a]Bontemps et al. (1996); except S2 from Ward-Thompson (1993).

[b]Taurus photometry from Kenyon et al. (1993); Ophiuchus photometry from Barsony et al. (1997).

Multiwavelength near-infrared images were obtained for eight YSOs using the HST/NICMOS camera from July to December 1997. The FWHM spatial resolution is $0.15'', 0.16''$, and $0.19''$ for the F160W, F187W, and F205W filters, which have central wavelengths of 1.60 μm, 1.87 μm, and 2.05 μm, respectively. The x and y plate scales were $0.0761''$ pix^{-1} and $0.0754''$ pix^{-1}, respectively, so that the chip size of 256×256 implies a $19.4''$ FOV. The dynamic range is typically 2000:1 in the reduced broadband images.

3. Protostar Images

Figure 1 displays NICMOS images for the six of eight sources which exhibit strong nebulosity. The structure is complex with the brightest emission close to the star. The protostar is visible toward all objects as a bright point source, appearing most strongly in the longest wavelength data (F205W) where the extinction is lowest. Toward IRS43 two pointlike sources show clearly the distinctive NICMOS diffraction pattern complete with main core, first Airy ring,

"dots", and diffraction spikes. The following sections describe the sources in pedagogical order. A more detailed description is available in Terebey et al. (2000a).

3.1. IRAS16244-2432/IRS44/L1681B/YLW16A – A Protobinary

The HST/NICMOS image of IRS44 (Fig. 1) displays extensive reflection nebulosity with a few curving filaments. A magnified view of the bright central region (Fig. 2a) shows two point sources, resolving the source as a protobinary with $0.27'' = 43$ AU (PA 81°) separation. The primary is detected at all three wavelengths. The secondary is visible only in the longest 2.05 μm wavelength; the two shorter wavelength images define a dust absorption lane which extends roughly north-south. The images illustrate IRS44 as a protostar, caught during the dynamical collapse phase, which is actively forming a binary from the surrounding gas.

The standard interpretation for a dust lane invokes a circumstellar disk, seen edge-on to produce the relatively narrow ($\sim 0.3''$) absorption feature. However, the north-south orientation of the dust lane is puzzling. CO and H_2O maser interferometry data (Terebey, Vogel, & Myers 1989, 1992), which show a jet with overlapping red and blue shifted CO gas, also suggest a highly inclined system. However the observed outflow axis extends north-south, parallel rather than perpendicular to the dust lane. Outside the HST/NICMOS FOV the nebulosity is decidedly brighter on the western edge, leading Lucas & Roche (1998) to experiment with nonaxisymmetric density models. On a $\sim 20''$ scale (outside the NICMOS FOV) the source is a YSO triple system. The misaligned dynamical axes, nonaxisymmetric nebulosity, and multiplicity on a larger scale suggest density inhomogeneities which may lead to time varying dynamical structure.

3.2. IRAS04361+2547/TMR-1 – Protobinary

The nebulosity seen toward TMR-1 (Fig. 1) presents a very complex structure, which is difficult to interpret in terms of an axisymmetric model. Mixed in are faint diffraction spikes, seen at similar position angle as for IRS43 (Fig. 1). Ground-based data show large scale nebulosity at PA $\sim$ -40°which is associated with a CO outflow (Terebey et al. 1990; Lucas & Roche 1998; Hogerheijde et al 1998). In Figure 2b the zoomed view of the bright central regions shows this source is a protobinary with $0.31'' = 43$ AU (PA 19°) separation surrounded by nebulosity. Both objects exhibit the first diffraction ring and are detected at all three wavelengths. A prominent narrow filament extends southeast from the protostar to a point source TMR-1C located $10''$ away. We previously suggested that the morphology of TMR-1C could plausibly be explained as a young brown dwarf which had been ejected from the protobinary system a few thousand years ago (Terebey et al. 1998, 2000b). Follow-up low-resolution Grism spectroscopy constrains the temperature of TMR-1C to be greater than 2700 K, which is hotter than predicted by theoretical models. However the models are not expected to apply to objects less than one million years old, leaving some ambiguity about the result. A higher resolution (R $\sim$ 500) spectrum capable of detecting photospheric lines would better test whether the object is a background star.

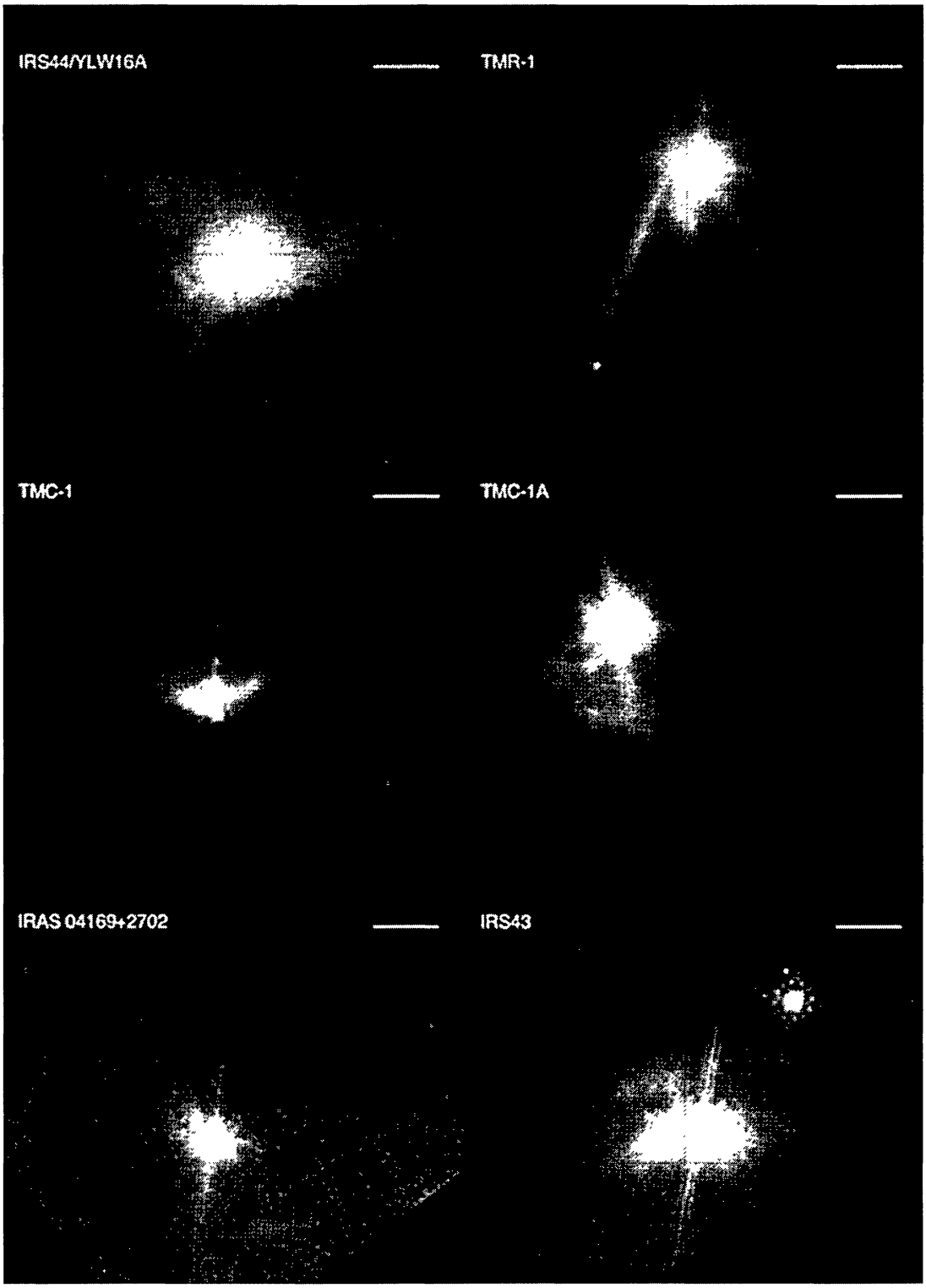

Figure 1. HST/NICMOS images of protostars show complex nebulosity, binary protostars and circumstellar absorption in the 19.4″ FOV. Scale bar is 3″ ∼ 450 AU. Log stretch; North - top; East - left.

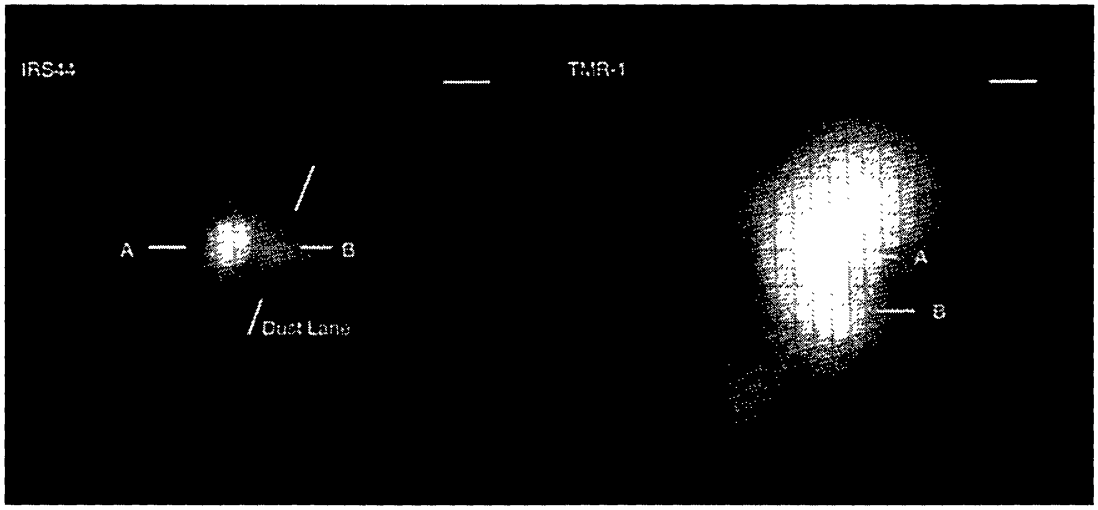

Figure 2. Expanded view of inner region shows the newly detected protobinary systems. Scale bar is $0.3'' \sim 45$ AU. Left panel: One component of the IRS44 protobinary is visible only in the F205W filter, presumably due to high extinction which blocks its light at shorter wavelengths. Display uses linear stretch. Right panel: TMR-1 shows two components complete with first Airy diffraction rings, plus bright nebulosity to NW. Display uses log stretch.

3.3. IRAS04381+2540/TMC1 – Jet Source with Wide-Angle Wind

The source TMC1 (Fig. 1) has extended emission covering most of the FOV; the lowest contours define a beautiful wide-angle conical reflection nebulosity, one-sided, whose central star is seen at the southern apex. Previous NIR and CO data show a wide-angle biconical outflow which extends north-south; the derived inclination is 40–70 degrees (Chandler et al. 1996). NIR scattering models predict the one-sided shape for moderate inclination sources (Whitney et al. 1993); the blue-shifted northern lobe is nearer, and hence clearly visible, while the red-shifted southern lobe is farther away, and completely extincted by the intervening circumstellar disk/ flattened infall envelope.

A well defined jet extends nearly $4''$ north from the source. There is only F160W data for this, our faintest source. Presumably the emission is due to Fe[II] line emission at 1.64 μm, contained within the F160W passband. The jet appears unresolved in the perpendicular direction at $0.15'' = 21$ AU resolution. The jet is not perfectly straight; a line drawn back towards the source does not point directly toward the protostar, but in between the protostar and the bright neighboring cometary clump. It is tempting to speculate that the comet shaped clump represents a second embedded star, but these data are not definitive.

Despite the large numbers of known jet sources and molecular outflow sources there are few examples of young stars simultaneously showing both wide-angle outflows and jets. The exceptions are the well known class I source L1551-IRS5 (Davis et al. 1995) plus possibly the source FS TauB (Eisloffel & Mundt 1998). However due to confusion with a nearby star the spectral energy distribution and classification of FS TauB are not well known. By contrast, TMC1 is

isolated and well characterized as a typical class I protostar. It makes a striking case for a unified theory which simultaneously connects jets with wide-angle outflows.

3.4. IRAS04365+2535/TMC1A – Infall Streamers

Ground-based images show a beautiful biconical nebulosity that extends from northwest to southeast whose derived source inclination is 40-70° (Chandler et al. 1996). NIR scattering models predict the source shape to be biconical above 60° inclination (Whitney et al. 1993). The high spatial resolution of the HST/NICMOS data (Fig. 1) reveals complex structure, but at the lowest intensity levels (not shown) the data are consistent with the expected hour-glass shape. The southern lobe appears much fainter than the northern lobe, evidence for absorption by the intervening circumstellar disk/flattened infall envelope. This pattern is consistent with the CO outflow data which show the northern lobe to be blue-shifted and therefore presumably closer and less obscured. The bright central region is not pointlike ($\sim 0.4''$), but instead is triangular in shape, and may represent a partially resolved triple protostar system. However the two northern components sit within nebulosity; higher spatial resolution is needed to settle the issue.

Outside the central region is an arc of emission which extends northeast, then curves to the north. This curving filament can be followed about $2'' = 300$ AU outwards before merging into the surrounding nebulosity. A second fainter arc, barely visible in the chosen stretch, starts near the same apparent position, but follows a less curved track outward. By their morphology these curved filaments do not appear to be part of the outflow structure. Instead we postulate that they are part of the infall envelope, streamers of overdense infalling material that follow the curved elliptical streamlines of the collapsing gas, curved by conservation of angular momentum as the gas nears the circumstellar disk.

3.5. IRAS04169+2702/B213 – Stellar Wind Bubbles/Loops

The structure in the reflection nebulosity around IRAS04169+2702 (Fig. 1) appears primarily related to the outflow. In addition to the stellar PSF there is also very low level extended emission $\sim 10''$ covering most of the lower right hand quadrant; it is not a flat fielding error or a chip artifact, but instead represents a wide-angle conical reflection nebulosity which extends southwest from the star (Tamura et al. 1991; Whitney et al. 1997). The nebulosity coincides with the blue-shifted CO lobe (Bontemps et al. 1996), as if illuminating the near-side outflow cone. The position angle of the CO outflow axis is $\sim 45°$ while perpendicular to that axis is a ridge of dense, possibly infalling gas (Ohashi et al. 1997). At a faint level (not visible in Fig. 1) the nebulosity shows two 'loops' of emission. Northeast of the protostar is a $\sim 2''$ filled loop while to the southwest is a slightly larger $\sim 3''$ unfilled loop. Both features lie near the CO outflow axis which suggests the NIR loops are features associated with the outflow rather than infall. Similar loop features are seen toward the source CoKu Tau1 (Padgett et al. 1999).

3.6. IRS43/Oph F – Circumstellar Disk Around a more Evolved Source

Towards IRS43 (Fig. 1) the central star is easily visible, while a dark dust absorption lane is flanked by nebulosity. A second young star, GY263 lies in the field; its association with IRS43 is unknown. The scattered light morphology is similar to HH30 (Burrows et al. 1996). Although not seen precisely edge-on as HH30, IRS43 also appears to be highly inclined. The fact the central star exhibits strong PSF features at all wavelengths indicates there is relatively less extended dust (reflection nebulosity) as well as a lower optical depth to the star than the other objects in our sample. By analogy with HH30 we propose IRS43 has a circumstellar disk but has only a weak infall envelope, so the NIR appearance is primarily that of an inclined disk seen in absorption, whose surface is illuminated by the scattered photons. Although IRS43 is designated a class I protostar, the weak infall envelope suggests a more advanced evolutionary stage than our other sources. This source is unusual in that an X-ray flare was seen toward it (Grosso et al. 1997; Montmerle et al 2000; Tsuboi et al. 2000).

4. Summary

We present HST/NICMOS images of six protostars made with 0.15″, or 20 – 25 AU, spatial resolution. The sample of class I sources represents protostars viewed during the main accretion phase. For typical protostars the gas is too cold for the dense cores to be pressure supported on scales of $3'' \sim 500$ AU, implying these images are sensitive to gas that is in motion, whether due to collapse, outflow, or rotation. The high spatial resolution HST/NICMOS images offer abundant evidence of features related to dynamical collapse. Binary protostars are seen, presumably forming from the surrounding dense gas in IRS44 and TMR-1 and having separations of $0.3'' = 45$ AU. In the source TMC1A streamers of material curve/flow into the central regions: we suggest these may represent overdense streamers of infalling gas. The protobinary IRS44 exhibits a dust absorption lane which is parallel rather than perpendicular to the outflow axis, offering another indicator of dynamically changing structure.

In an HST/NICMOS survey of edge-on YSO systems, Padgett et al. (1999) find strong evidence for dust absorption lanes. Despite less favorable source inclinations, these six protostars also show evidence for dust absorption lanes or heavily extincted outflow lobes. The absorption arises either from a circumstellar disk, or alternatively, from the flattened dense equatorial regions of the infall envelope.

The source TMC1 shows a wide-angle outflow, and simultaneously a narrow jet, unresolved in the perpendicular direction, extending nearly 4″ from the central star. This rare combination also occurs in L1551-IRS5, and the more recently discovered FS TauB. This places very strong constraints on theoretical models of protostellar outflows.

In summary, these stunning NICMOS HST images provide a new view of the gravitational collapse phase, showing complex but understandable structure in these $1 - 3 \times 10^5$ yr old protostars.

Acknowledgments. S. Terebey thanks and acknowledges NASA for support from the NASA Origins of Solar Systems Program under contract NASW-97009, and from grant GO-07325.01-96A through the Space Telescope Science Institute, which is operated by the Association of Universities for Research in Astronomy, Inc., under NASA contract NAS5-26555. This work was carried out in part at the Jet Propulsion Laboratory, operated by Caltech under contract for NASA.

References

Barsony, M., Kenyon, S. J., Lada, E. A., & Teuben, P. J. 1997, ApJS, 112, 109

Bate, M. R. 1997, MNRAS, 285, 16

Bodenheimer, P., Ruzmaikina, T., & Mathieu, R. D. 1993, in Protostars and Planets III, Eds. E. H. Levy & J. I. Lunine (Tucson: Univ. of Arizona), 367

Bonnell, I. A., & Bate, M. R. 1994, MNRAS, 271, 999

Bontemps, S., André, P., Terebey, S., & Cabrit, S. 1996, A&A, 858

Boss, A. P. 1986, ApJS, 62, 519

Boss, A. P. 1995, RevMexAA, 1, 165

Burrows, C. J., Stapelfeldt, K. R., Watson, A. M. et al. 1996, ApJ, 473, 437

Chandler, C. J., Terebey, S., Barsony, M., Moore, T. J. T., & Gautier, T. N. 1996, ApJ, 471, 308

Davis, C. J., Mundt, R., Ray, T. P., & Eisloffel, J. 1995, AJ, 110, 766

Eisloffel, J. & Mundt, R. 1998, AJ, 115, 1554

Grosso, N., Montmerle, J., Feigelson, E. D., André, P., Casanova, S., & Gregorio-Hetem, J. 1997, Nature, 387, 56

Heyer, M.H., Ladd, E.F., Myers, P.C. & Campbell, B. 1990, AJ, 99, 1585

Hogerheijde, M. R., Van Dishoeck, E. F., Blake, G. A. & Van Langevelde, H. J. 1998, ApJ, 502, 315

Kenyon, S. J., Calvet, N., & Hartmann, L. W. 1993, ApJ., 414, 676

Lada, C. J. 1987, in Star Forming Regions, eds. M. Peimbert & J. Jugaku, (Dordrecht: Reidel), p. 1

Lucas, P. W. & Roche, P. F. 1997, MNRAS, 286, 895

Lucas, P. W. & Roche, P. F. 1998, MNRAS, 299, 699

Montmerle, T., Grosso, N., Tsuboi, Y., & Koyama, K. 2000, ApJ, 532, 1097

Ohashi, N., Hayashi, M., Ho, P. T. P., Momose, M., Tamura, M., Hirano, N., & Sargent, A. I. 1997, ApJ, 488, 317

Osterloh, M., & Beckwith, S. V. W. 1995, ApJ, 439, 299

Padgett, D. L., Brandner, W., Stapelfeldt, K. R., Strom, S. E., Terebey, S., & Koerner, D. 1999, AJ, 117, 1490

Shu, F. H., Adams, F. & Lizano, S. 1987, ARA&A, 25, 23

Tamura, M., Gatley, I., Waller, W. & Werner, M. W. 1991, ApJ, 374, L25

Terebey, S., Beichman, C. A., Gautier, T. N., & Hester, J. J. 1990, ApJ, 362, L63 759

Terebey, S., Van Buren, D., Hancock, T., Padgett, D. L., & Brundage, M. 2000a, in preparation

Terebey, S., Van Buren, D., Padgett, D. L. P., Hancock, T. J., & Brundage, M. 1998, ApJL, 507, L71

Terebey, S., Van Buren, D., Matthews, K. & Padgett, D. L. P., 2000b, AJ, 119, 2341

Terebey, S., Vogel, S. N., & Myers, P. C. 1989, ApJ, 340, 472

Terebey, S., Vogel, S. N., & Myers, P. C. 1992, ApJ, 390, 181

Tsuboi, Y. et al. 2000, ApJ, 532, 1089

Ward-Thompson, D. 1993, MNRAS, 265, 493

Whitney, B. A. & Hartmann, L. 1993, ApJ, 402, 605

Whitney, B. A., Kenyon, S. J., & Gomez, M. 1997, ApJ, 485, 703

4. Origin of the Initial Mass Function